Jurnal Ni-dipend TiO2

by Jacson Morin

Submission date: 19-Apr-2023 05:26PM (UTC+0900)
Submission ID: 2069172425
File name: ok_Jurnal_Ni-dipend_TiO2.pdf (2.01M)
Word count: 6003
Character count: 28008

RJC

RASĀYAN *J. Chem.*
Vol. 13 | No. 2 |1225-1237| April - June | 2020
ISSN: 0974-1496 | e-ISSN: 0976-0083 | CODEN: RJCABP
http://www.rasayanjournal.com
http://www.rasayanjournal.co.in

ACTIVITY OF Ni-DOPED TiO_2/CERAMIC TUBE AS A SENSOR OF CO GAS FROM MOTOR VEHICLES

Jacson Victor Morin[1,3], Endang Tri Wahyuni[1,*], Adhitasari Suratman[1] and Ahmad Ashari[2]

[1]Chemistry Department, Faculty of Mathematics and Natural Sciences, Gadjah Mada University, Yogyakarta, Indonesia

[2] Department Computer Science and Electronics, Faculty of Mathematics and Natural Sciences Gadjah Mada University, Yogyakarta, Indonesia

[3]Chemistry Department, Faculty of Mathematics and Nature Sciences Papua, University, Papua Barat, Indonesia

[*] E-mail: endang_triw@ugm.ac.id

ABSTRACT

The activity of Ni-doped TiO_2 was investigated as a CO gas sensor. The material used as a sensor substrate is made of ceramic tubes that can withstand the heat of more than 1,000 ºC. Ni-TiO_2 sensor thin layer was made by dip-coating technique. Ni-doped TiO_2 solution was prepared from TiO_2 and nickel metal. The calcination temperature variations of 350 ºC (SOL1), 450 ºC (SOL2), 550 ºC (SOL3), and 650 ºC (SOL4) were used in determining the optimal conditions of Ni sensor materials doped with TiO_2. The characterization of the synthesized Ni-TiO_2 semiconductor using UVDRS, XRD, SEM-EDX, and FT-IR. The SOL2 showed the smallest bandgap of 2.86 eV as the UVDRS results. The XRD results showed that doped Ni particles in SOL2 sample have an anatase phase and crystal size of 15.528 nm. The SEM-EDX results showed the distribution of Ti and Ni of SOL2 sample were 43.92% and 4.27%, respectively. The SOL2 sample morphology exhibited a spherical shape and was more uniform than the SOL4. The performance of SOL2 sensor activity showed the operating temperature at 250 ºC with the CO gas concentrations up to 1,000 ppm.

Keywords: Ni-doped TiO_2, Carbon Monoxide, Dip Coating

INTRODUCTION

At present, air pollution is a problem that requires special attention. Some gases that cause air pollution include CO_2[1], CO[2], NOx[3], PM_{10}, and $PM_{2,5}$[4]. Most of the problems in air pollution were caused by motorized vehicles[5]. One way to monitor pollutant gas emissions in the environment is to find out the amount of gas produced in motorized vehicles so that periodic maintenance can be carried out on vehicles.

Carbon monoxide gas was a gas studied by researchers because it was dangerous and it was estimated that there are cases of CO poisoning every year, based on emergency department visits, were 50,000 (16.0 cases per 100,000 population). Research shows a reduction in the number of CO gas deaths, most recently found to be 1,319 in 2014, from an estimated 2,700 in mid-2000[6].

There are two ways to measure the level of monoxide gas, namely using the classical method and instruments. The use of classical methods still has disadvantages because it still uses chemical solutions as a gas absorber in the air and requires a long time. Modern methods that use gas sensor instruments have been widely used because they are more practical. Several studies have developed the manufacture of CO gas sensors, including from aluminium-doped CuO[7]; CO gas sensor from tetragonal graphene[8]; CO gas sensors from palladium and thin oxide nanocomposites[9]; CO gas sensor from thin oxide[10]; CO gas sensors from gold and thin dioxid[11]; CO gas sensor from thin layer ZnO[12]; CO gas sensor from $BaSnO_3$[13]; CO gas sensor from Ni, Zn doped SnO_2[14].

Rasayan J. Chem., 13(2), 1225-1237(2020)
http://dx.doi.org/10.31788/RJC.2020.1325720

Metal doping into semiconductor materials has been extensively studied, such as Cr metal-doped TiO_2 as a gas sensor[15]; CO gas sensors made from Ta/Nb which are doped with titania[16]; manufacture of gas sensors from titanium oxide doped vanadium and tantalum materials[17]. The use of doping in semiconductor material to make the sensor more sensitive, selectivity, and low temperature, metal doping into the semiconductor material will produce a suitable band gap value as a sensor and decrease the value of the sensor resistance when detecting gases in the air[18].

This research studied the synthesis of carbon monoxide gas sensors from nickel metal, which doped into titanium oxide semiconductor material using the dip-coating method. The process of making CO gas sensors using the dip-coating method.[19-21] By making the sol-gel solution. The dip-coating method has been widely used and has advantages, including having a simple and inexpensive technique that could be used in mass sensor production.[22] The Dip-coating technique contains three parameters consisting of (i) immersion and residence time, (ii) solvent deposition and flow, and (iii) evaporation. These three parameters must be adjusted when coating thin film.[23]

The shape of the TiO_2 doped Ni sensor is tubular.[24-30] The advantages of tubular sensors are that the resulting pen will be evenly distributed, and the sensitivity is very high[31]. The characteristics of the TiO_2 doped Ni material were carried out with XRD, UV-Vis, SEM and sensor resistance measurements using a multimeter. The results of the reading of the sensor in the form of ppm units derived from changes in resistance and voltage scale by the Arduino system.[32-36]

EXPERIMENTAL

Synthesis of Ni-Doped TiO_2

A thin layer of TiO_2 doped with Ni metal was deposited on the surface of the substrate by the dip-coating method. The substrate used was the Al_2O_3 ceramic tube. The substrate was cleaned for 2 hours in an ultrasonic bath (Model Starsonic 60) with ethanol and then dried in an oven at 80 ºC for 15 minutes. For coating ceramic substrates with nickel-doped titanium dioxide. Nickel solution was made from $NiCl_2 6H_2O$ (Sigma Aldrich, 99.9%) 0.7 mol and mixed with titania sol-gel solution. The titania-sol form was prepared as follows: 30 mL titanium (IV) isopropoxide (TTIP) (Merck, 98%) was dissolved in 10 ml of isopropanol (Merck, 99.5%). Then the prepared solution was stirred using a stirrer (800 rpm) for 8 hours. After mixing the solution, nitric acid (HNO_3) (Merck, 65%) or acetic acid (CH_3COOH) (Merck, 95%) was added as a stabilizer, and methylcellulose (MC) (Merck, 2 Wt%) was used as an emulsifier. The ceramic tube substrate was dipped into a solution of TiO_2 doped Ni sol-gel with the immersion stage. The first step is immersion for 5 minutes, then in the oven at 115 ºC cooled and in the second stage dipped for 15 minutes and in the oven at 115 ºC and in the third stage dipped for 25 minutes and heated at 115 ºC. After that, it is entered into the maffle furnace with different temperature variations for each sample for 1 hour as in Table -1.

Table -1: Variation of Substrate-Solgel Heating Temperatures

Sample	Temperature(ºC)
SOL 1	350
SOL 2	450
SOL 3	550
SOL 4	650

Characterization of Ni-Doped TiO_2

The synthesized Ni-dopedTiO_2, characterized, tested for photocatalyst activity using UVDRS, and obtained the optimum thin layer with these parameters, determined the band value energy gap. The thin layer of crystalline Ni-doped TiO_2 synthesized transmission measured in the wavelength range of 300-700 nm. The measurement results obtained transmittance value is proportional to the wavelength which is absorbed by a thin layer of TiO2. The obtained value of the Ni-doped TiO_2 thin layer transmittance will be processed using the Kubelka Munk equation for calculating the bandgap energy value. The Ni-dopedTiO_2 crystal structure was identified by XRD (XRD, Philips PW 1840; 40 kV and 30 mA generator settings; Cu anode material). The orientation of the curve is determined by comparing the relative

intensity based on the JCPDS card[37]. The phase of the sample can be calculated from the peak anatase intensity (101) as:

$$W_A = \frac{K_A A_A}{K_A A_A + A_R + K_B A_B} \quad (1)$$

Where, WA represents the anatase mass fraction. AA, AB, and AR were the integrated intensity of the anatase peaks (101), brookite (121), and rutile (110), respectively. KA and KB are two coefficients values are 0.886 and 2.721, respectively. With Eq. 1, the phase content in the TiO_2 sample could be calculated (JCPDS Powder Diffraction File, Cards 21-1272, 21-1276, 29-1360). The average crystal size of the anatase was determined according to Scherrer's equation using FWHM data from each phase [38, 39, 40, 41, 42, 43].

Nickel-doped TiO_2 deposited on the surface of the substrate was analyzed by scanning electron microscope (SEM, Hitachi S-3400 N)[44,45] using a secondary electron detector. Energy-dispersive X-ray spectroscopy (EDS, Bruker Quad 5040)[46,47] was used for elemental composition analysis and element mapping from TiO_2 films. Particle size and morphology confirmed through SEM were done with a 30 kV JEOL electron microscope transmission (sputtering using platinum). Fourier-Transform Infrared Spectroscopic (FTIR) analysis was performed using Perkin Elmer Spectrum Version 10.4.00[48]; The UV-vis spectrum was recorded through the Vary Cary Bio 50 spectrometer.[49,50]

The Performance of the Sensor Activity Test

Figure -1 shows the schematic diagram of a gas sensor. Static processes were used to test sensor properties in the 10 L chamber. Test reactor conditions were prepared by injecting a saturated CO gas amount into the 10 L chamber, where a vacuum pump was installed to homogenize the CO gas in the reactor chamber. The gas sensor is fed into the test reactor together with a calibrated gas detector. The gas contained in the reactor tube will be detected and controlled by the system, and the gas sensor resistance in the clean air (Ra) together with the target gas (Rg) is monitored in real-time respectively. The response of the gas sensor is defined as Ra/Rg to reduce CO gas. After testing, the reactor chamber is cleaned by vacuuming it for 20 minutes to reset the next test.

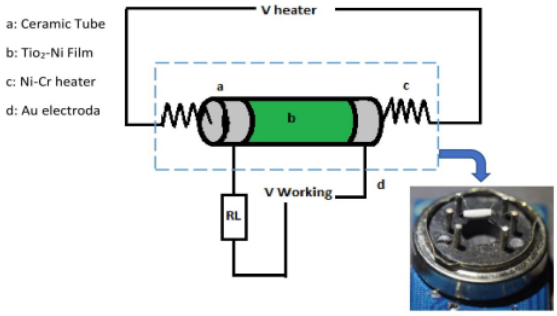

Fig.-1: Schematic of a Ni-doped TiO_2 Gas Sensor

The Ni-doped TiO_2 sensor was connected to the Arduino system with an Atmega microcontroller (purchased from Amazon.com) that can convert resistance readings into units of concentration (ppm). Arduino Uno software version 1.8.9 and Parallax. DAQ was needed in processing data from sensor readings.

RESULTS AND DISCUSSION

Physical Properties of Synthesized Ni-Doped TiO_2

Based on the results of UVDRS analysis and using the Kubelka Munk equation, the bandgap values obtained are shown in Table-2.

Table -2 shows the energy values of the Ni-doped TiO_2 doped Ni bandgap. The energy of the Ni-doped TiO_2 band gap produced is relatively small compared to TiO_2 (3.28 eV) along with the addition to the variation of heating temperature in the Ni-doped TiO_2 sample. The optimum bandgap energy obtained in

this study was around 2.86 eV. TiO_2 doped Ni crystals were resulting in a decrease in the pit gap energy along with the addition of various variations in heating temperature.
Characterization by XRD method is carried out to obtain crystal structure information and crystallize size. The data obtained in the form of spacing, angular intensity 2 (Θ). In this study, standardized Ni-doped TiO_2 program was taken from JCPDS No.004-0850 (Nickel-metal), No. 89-5009 (titanium), No. 21-1272 (TiO_2 anatase), the crystallinity of Ni-doped TiO_2 has been compared with JCPDS No. 21-1271 is anatase in shape and its peak diffraction is shown at 25.1°, which is diffraction from (101) as shown in Figure -2.

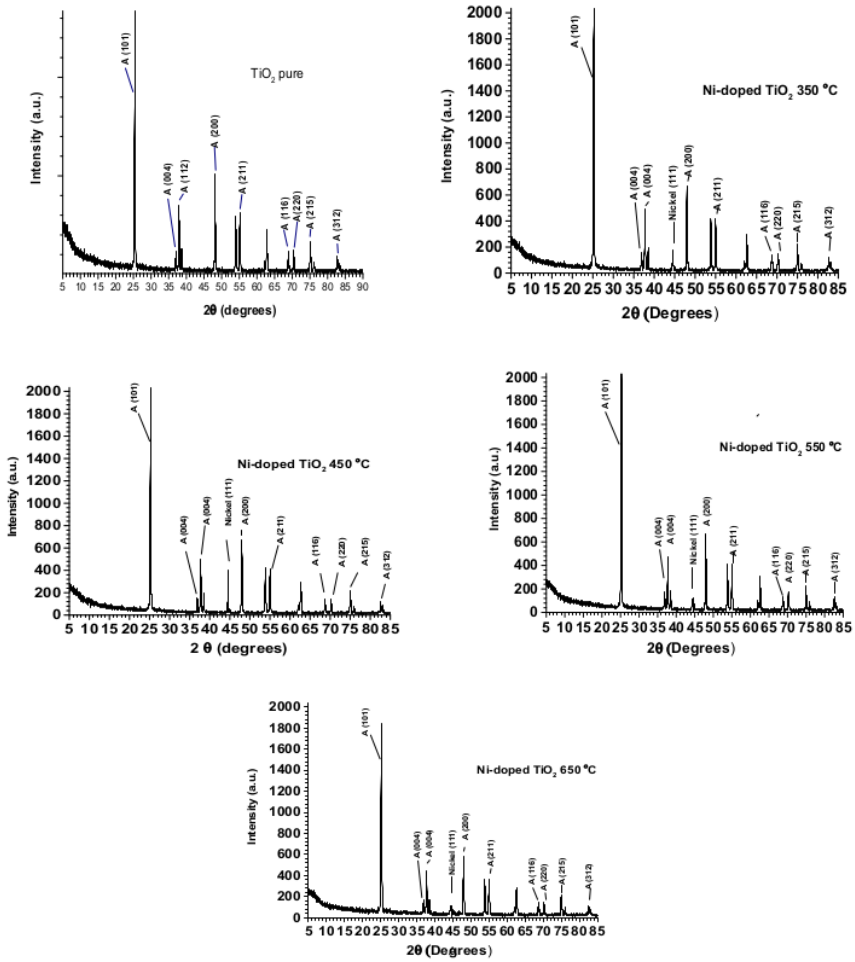

Fig.-2: XRD Diffraction Pattern at a Calcination Temperature of (a) TiO_2 pure, (b) 350ºC, (c) 450ºC (d) 550 ºC, and (e) 650 ºC

The XRD pattern shows that the addition of nickel variation does not affect the crystal phase between calcination variations of SOL1, SOL2, SOL3, and SOL4 with comparative data that is TiO_2 without nickel doping. Additional peaks appear at 2 (θ) 44,504 0 based on JCPDS No. 004-0850 shown in Figures b, c, d, and e shows the difference in nickel peak intensity due to differences in calcination temperature

differences. At calcination temperature, 450 ºC shows the high intensity of nickel-metal compared to 350 ºC, 550 ºC and 650 ºC. High calcination temperatures above 450 C cause the nickel-metal to evaporate and will reduce the intensity of nickel detected in the XRD pattern. This study shows the information value of 2 (θ) in the Ni-doped TiO_2 sample is following the Ni-doped TiO_2 in the comparison data and is an anatase crystal from diffraction (101) value of 2 (θ) which is 25.4°. Where each peak 2 (θ) has given the same or close results which is 25.4° (TiO_2 without doping Ni) to 25.3° (SOL1), 25.1° (SOL2), 25.2° (SOL3), and 25.1° (SOL4) and produces a lower crystal size of 47.074 nm (SOL1); 15.528 nm (SOL2); 39.546 nm (SOL3); and 64.172 nm (SOL4) (as shown in table - 3) compared to TiO_2 without Ni doping ie 40.15 nm. The results of this study indicate that the value 2 (θ) of the TiO_2 doped Ni data and the results of the variation of the research sample there is no significant difference, and both show the anatase crystal from diffraction (101).

Table-2: Results of the Ni-doped TiO_2 Bandgap Energy Calculation

No	Sample	E.g. (eV)
1	SOL1	3.01
2	SOL2	2.86
3	SOL3	2.9
4	SOL4	3.09

Table-3: Characterization of Data from TiO_2 Doped Ni

	Sample			
Analysis	350 ºC	450 ºC	550 ºC	650 ºC
K	0.89	0.89	0.89	0.89
Λ	0.154	0.154	0.154	0.154
2 Θ	25.284	25.1995	25.4237	25.1745
FWHM	0.1673	0.506	0.2007	0.1224
B (radian)	0.0029	0.0088	0.0035	0.0021
*D (nm)	47.074	15.528	39.546	64.172

The majority of the fractions that appear are anatase (101)[51-52] and The majority of the presence of these anatase fractions in all heating variations is due to the effect of HNO_3, CH_3COOH functioning as a hydrolysis catalyst in the manufacture of Ni-doped TiO_2. HNO_3 is a much stronger acid catalyst than CH_3COOH to crystallize the anatase phase. According to literature [53], the acid concentration is the dominant factor in the formation of the anatase phase. That's because H^+ ions rearrange amorphous aggregates to form anatase crystals. These results are below the results of the study, which claims that the anatase phase is stable in acidic solutions. The calculation results using the Scherrer equation, at a temperature variation of 450 ºC obtained a crystal size of 15,528 nm, which indicates that the surface area is getting bigger.

Characterization by using FTIR aims to find out the functional groups that compose the Ni-doped TiO_2 framework and to identify the presence of Ti-Ni vibrations as an indication of the formation of bonds between Ni and Ti, as a result of the addition of Ni metals. Figure -3 shows the FTIR spectrum of TiO_2 doped Ni in the range of 600–4000 cm^{-1} is a form of bending of the Ti-O vibration, which confirms the formation of metal-oxygen bonds[54]. The band located at 3450 cm^{-1} is associated with the stretching and bending vibrations of the O-H bond of H_2O absorbed on the surface of TiO_2, which is important in the activity of semiconductor gas sensors. The FTIR spectrum shows the intensity of the band shifting towards a lower direction after the doping of Ni metal and temperature variations.

FT-IR diagram of Ti-Ni showed the absorption peak at the wavenumber region of 400-1050 $cm^{-1,}$ which is a characteristic of O-Ti-O bonding, and there is a wavelength region of 1000-1700 cm^{-1} showing the presence of Ni-doped TiO_2 bonds[19]. The absorption band in the region of wave number 555.54 cm^{-1}

showed the Ti-O-Ti bond, which indicates the Ni interstitial TiO_2 doping bond model (nickel bound to oxygen).

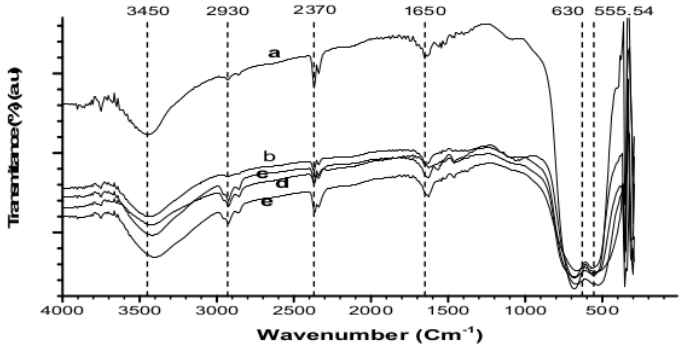

Fig.-3: FT-IR of TiO_2-Ni at (a) TiO_2 without Doping Ni Metal Calcination Temperature 450ºC, (b) Calcination 350ºC, (c) Calcination 450ºC, (d) Calcination 550ºC (e) Calcination 650ºC

The SEM-EDX study shown in Figs.-4 and -5, include TiO_2 pure and SOL1, SOL2, SOL3, and SOL4 samples. As can be seen, SOL1 and SOL3 samples were form non-agglomerations on the sensor surface. SOL2 and SOL3 samples have the best quality as a coated film because HNO_3 was strong enough to reduce the speed of hydrolysis and condensation of soles with the appropriate heating temperature. Therefore, at 450 ºC calcination appears as a regular solid structure, CH_3COOH caused phase separation in the sol and resulted in a cracked and rough texture on the sensor surface TiO_2[55].

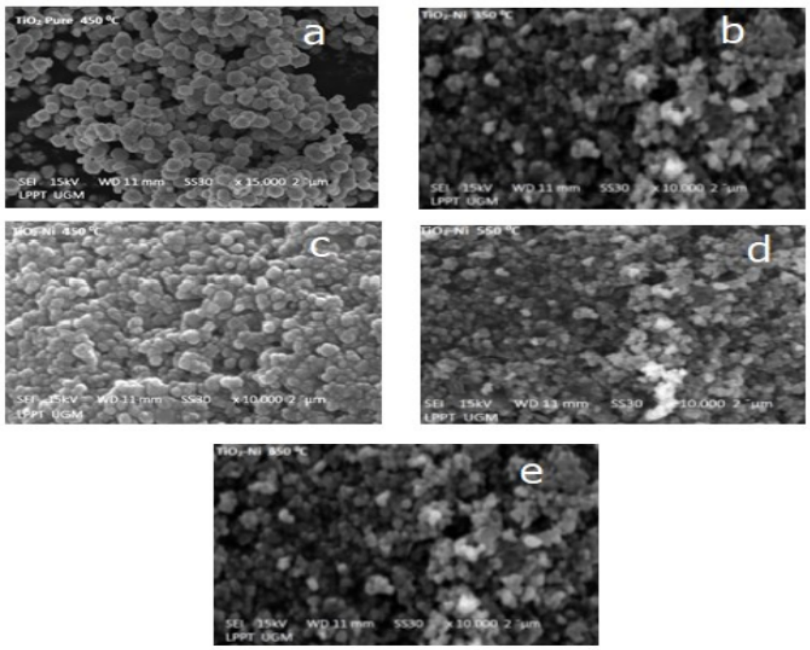

Fig.-4. SEM of (a) TiO_2 pure, (b) SOL1, (c) SOL2, (d) SOL3, and (e) SOL4

The presentation of Ni metal distribution is shown using EDX shown in Fig.-5, and From the distribution of Ni on the TiO_2 surface based on EDX, a table can be made showing the data in the form of mass units% of nickel metal, showed in Table -4.

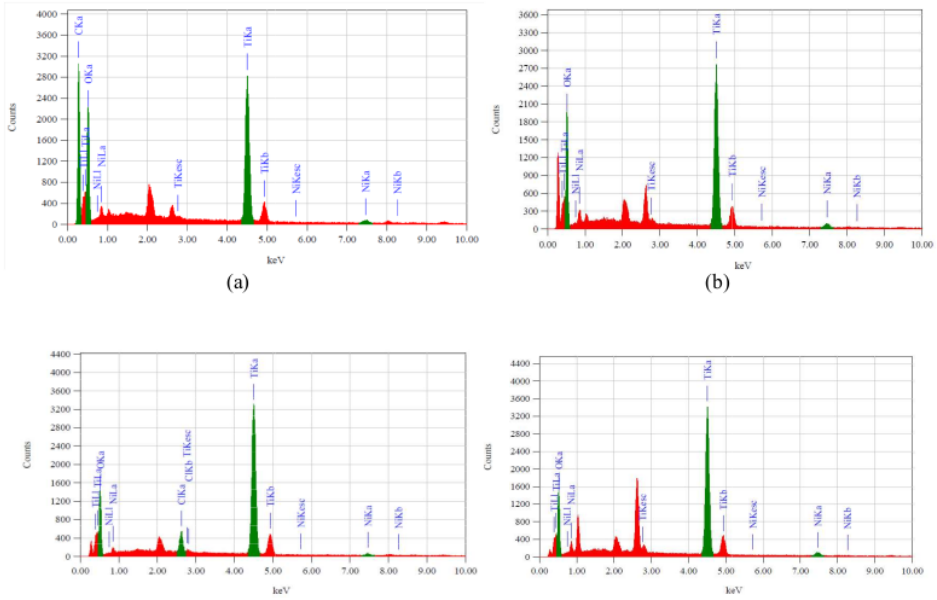

Fig.-5. EDX of: (a) SOL1, (b) SOL2, (c) SOL3, and (d) SOL4

Table-4: Distribution of Ni Metal on TiO_2 Surface from Calcination Temperature Variation

Variation of Calcination Temperature	Percent of Mass %
SOL1	1.53
SOL2	2.51
SOL3	1.27
SOL4	0.35

The Performance of the Sensor Activity Test

The manufacture of CO gas sensors based on characterization results of UV DRS, XRD, FTIR and SEM EDX for the SOL2 sample. Due to the bandgap generated is 2.86 eV as the optimal results as the semiconductor materials. Other than that, not only the morphology of Ni-doped TiO_2 was not agglomeration, but also the composition of Ti was 43.92%, and Ni was 4.27% so that Ni distribution will be evenly distributed on the surface and TiO_2 lattice.

Operating temperature is an essential parameter for semiconductor oxide sensors[56-57]. According to determine the optimal operating temperature, the sensor response depends on the measurement temperature with 500 ppm CO gas from the TiO_2-Ni sensor. Moreover, the results of this procedure were compared with the factory-manufactured MQ7 sensor and tested at temperatures ranging from 200 °C to 450 °C. The best response performance was shown at the operating temperature of 250 °C. Thus, the operating temperature of 250 °C was chosen as the optimal operating temperature for the study of Ni-TiO_2 based CO gas sensors. Figure -7 shows the sensor sensitivity versus CO concentration ranging from 25 to 1000 ppm at the operating temperature of 250 °C. Sensitivity increases when the concentration increases and the response of the TiO_2 doped Ni sensor are higher than the MQ7 sensor in all CO concentration test ranges.

Detection Limits (LoD) of CO Gas Sensor made From Ni-Doped TiO_2

The limit of detection of the Ni-doped TiO_2 sensor through data from the reading of the Ni-doped TiO_2 sensor is shown in Table-5 by comparing the data from the calibrated sensor reading.

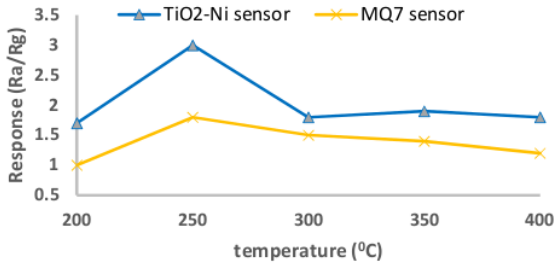

Fig.-6: Ra / Rg Response From CO Gas Sensors: (a) TiO_2-Ni, and (b) MQ7 Sensors

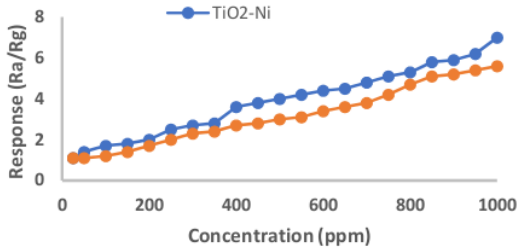

Fig.-7: Sensor Sensitivity Versus CO Concentration ranging from 25 to 1000 ppm at the Operating Temperature of 250 °C

Table-5: CO Gas Sensor Data from Calibrated Sensors and Ni-Doped TiO_2 Sensors

No.	Concentration of CO (ppm)	Readings From Calibrated Sensor (y_1)	Reading from the Sensor		
			Ni-doped TiO_2 (y_2)	(y_1-y_2)	(y_1-y_2)^2
1	0	0	0	0	0
2	2	2.4	1.89	0.51	0.2601
3	5	5.4	5.02	0.38	0.1444
4	10	9.6	9.87	-0.27	0.0729
5	15	14.9	14.9	0	0
6	25	25.03	25.05	-0.02	0.0004
7	30	33.01	29.8	3.21	10.3041
8	35	34.24	35.04	-0.8	0.64
9	40	42.05	42.4	-0.35	0.1225
10	45	43.7	44.8	-1.1	1.21
11	50	49.04	49.7	-0.66	0.4356
12	55	55.4	56.03	-0.63	0.3969
13	60	58.6	60.07	-1.47	2.1609
14	65	64.2	64.8	-0.6	0.36

15	70	69.8	70.5	-0.7	0.49
16	75	76.2	74.7	1.5	2.25
17	80	79.8	79.7	0.1	0.01
18	85	85.2	85.06	0.14	0.0196
19	90	89.6	89.11	0.49	0.2401
20	95	94.7	97.2	-2.5	6.25
21	100	98.7	100.06	-1.36	1.8496

$SD = S_{y/x} = \sqrt{\frac{27.2171}{19}}$

$SD = 1.197$

$Y_{LoD} = 3.SD + a$

$= 3\,(1.197) + 0$ (a = 0, because the resulting linear equation y = 1.0034x)

$Y_{LoD} = 3.591$ ppm

Determination of linear equations derived from the graph between CO gas concentrations versus CO gas concentrations read by a calibrated sensor. as shown in Fig.-8.

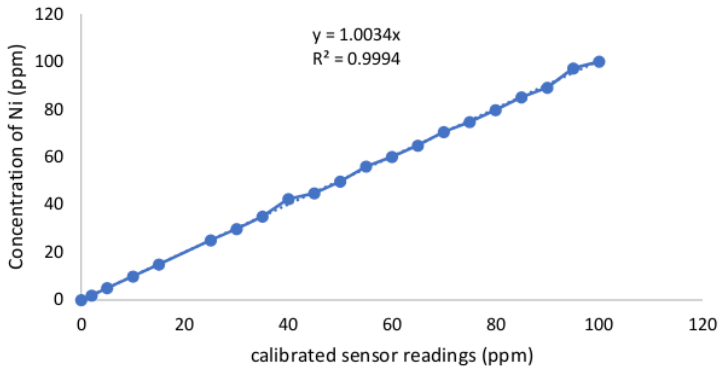

Fig.-8: Linear Regression Curve of CO Gas Concentration Vs CO Gas Concentration of the Calibrated Sensor

After the YloD value is known, then it is substituted in the equation, y = ax + b

YLoD = 1.0034x + 0
3.591 ppm = 1.0034x
X = 3.6 ppm
X = LOD
The detection limit for CO gas sensors made from TiO_2-Ni is 3.6 ppm

Application of Ni-Doped TiO_2 Sensors in Motor Vehicles

The performance test of the Ni-doped TiO_2 gas sensor in car exhaust exhibited in Fig.-8. The results showed high sensitivity and average CO gas measurement in cars under 50 ppm. The reading of the TiO_2-Ni sensor is converted with the Arduino system, which changes the resistance reading into ppm units and is processed using the Parallax DAQ software. The measurement results shown in Figure -10, there are two graphs a and b. The chart shows the first gas sensor reading of the car engine is turned on and graph b the second gas sensor reading after the engine has been turned off for 20 minutes and turned on again.

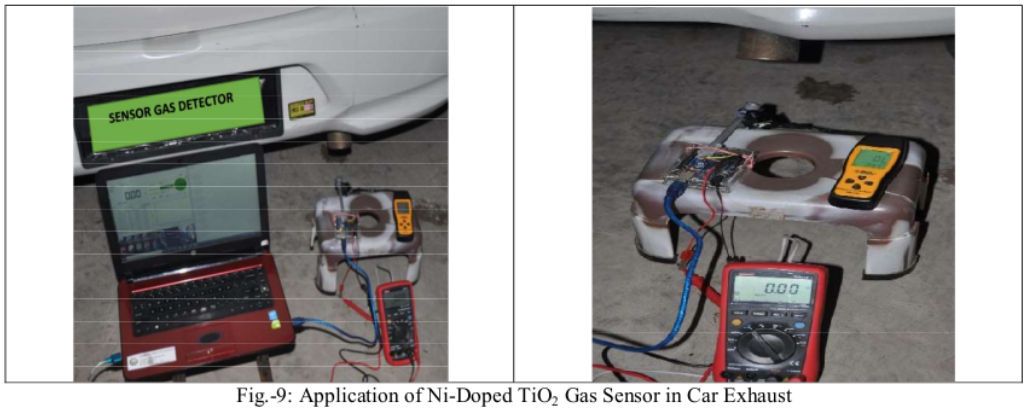

Fig.-9: Application of Ni-Doped TiO_2 Gas Sensor in Car Exhaust

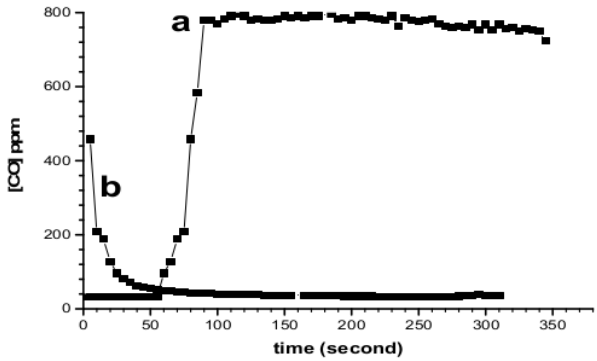

Fig.-10: (a) First Reading of Car Exhaust, (b) Second Reading of Car Exhaust after Cleaning.

At the first stage of reading, CO levels are still very high when the sensor responds to gas at minutes 60 to 345 by showing the figure 724 ppm shown in Figure 10(a). Figure 10(b) showed CO levels in car exhaust after the engine was cleaned, around 458 ppm in the first 5 seconds to 115 seconds around 39 ppm CO.

CONCLUSION

The CO gas sensor from Ni-doped TiO_2 with an anatase crystal size of 15.528 nm was deposited on a ceramic substrate tube to improve the properties of the gas sensor. The gas sensor activity and the titania thin film texture are prepared by the sol-gel method in which there is a solvent acting as a stabilizer. Calcination temperatures of 450 °C and HNO_3 cause optimal band gap values for semiconductor materials. HNO_3 acts as a stabilizer in the sol-gel from the anatase crystallization stage. The Arduino microcontroller, which is used to change the resistance of Ni-doped TiO2 sensors, is operated efficiently so that the calibration process can be carried out correctly. The ability of Ni sensors doped with TiO_2 is sensitive compared to factory production sensors (MQ7) with a LOD value of 3.6 ppm, so that TiO_2 doped semiconductors Ni can be used as a sensitive and efficient carbon monoxide gas sensor.

ACKNOWLEDGMENT

The author would like to thank the Department of Chemistry, Gadjah Mada University, and Indonesia Endowment Fund for Education (LPDP-BUDIDN), for providing funds and facilities for this research.

REFERENCES

1. G. Năstase, A. Şerban, A.F. Năstase, G. Dragomir, A.I. Brezeanu, *Atmospheric Environment* **184**, 292(2018), **DOI:**10.1016/j.atmosenv.2018.04.034
2. H.C. Ong, T.M.I. Mahlia, H.H. Masjuki, *Renewable and Sustainable Energy Reviews,* **5(8)**, 3516(2011), **DOI:**10.1016/j.rser.2011.05.006
3. J. Buekers, M. Van Holderbeke, J. Bierkens, L. Int Panis, *Transportation Research Part D: Transport and Environment,* **33,** 26(2014), **DOI:**10.1016/j.trd.2014.09.002
4. M.J.S. Fernandes, C.O. Carletti, L.F. Sierra de Araújo, R.C. Santos, J. Reis, *Revue Neurologique,* **175(10)**, 604(2019), **DOI:**10.1016/j.neurol.2019.07.013
5. M.F. Hung, C.T. Chang, D. Shaw. *Journal of Cleaner Production* **227**, 566(2019), **DOI:**10.1016/j.jclepro.2019.04.163
6. J.J. Rose, L. Wang , Q. Xu, C.F. McTiernan, S. Shiva, J. Tejero, M.T. Gladwin, *American Journal of Respiratory and Critical Care Medicine,* **195(5)**, 596(2017), **DOI:**10.1164/rccm.201606-1275CI
7. R. Molavi , M.H. Sheikhi , *Materials Letters,* **233(3)**, 74(2018), **DOI:**10.1016/j.matlet.2018.08.087
8. A. Bandyopadhyay, S. Paria, D. Jana, *Journal of Physics and Chemistry of Solids,* **123,** 172(2018), **DOI:**10.1016/j.jps.2018.07.015
9. S. Absalan, S. Nasresfahani, M.H. Sheikhi, *Journal of Alloys and Compounds,* **795**, 79(2019), **DOI:**10.1016/j.jallcom.2019.04.187
10. PP. Tsai, I.C. Chen, M.H.Tzeng, *Sensors and Actuators: B. Chemical*, **25(1)**, 537(1995), **DOI:**10.1016/0925-4005(95)85116-X
11. S. Wang ,Y. Zhao, J. Huang , Y. Wang, S. Wu, S. Zhang, W. Huang, *Solid-State Electronics,* **50(11)**, 1728(2006), **DOI:**10.1016/j.sse.2006.10.002
12. A. Paliwal , A. Sharma, M. Tomar , V. Gupta, *Sensors and Actuators, B: Chemical,* **250**, 679(2017), **DOI:**10.1016/j.snb.2017.05.064
13. U. Lampe, J. Gerblinger, H. Meixner, *Sensors and Actuators B: Chemical,* **25(1)**, 657(1995), **DOI:**10.1016/0925-4005(95)85145-3
14. Q. Zhou, W. Chen, L. Xu, K. Rajesh, Y. Gui, Z. Zhao, C. Tang, S. Zhu, *Ceramics International,* **44(4)**, 4392(2018), **DOI:**10.1016/j.ceramint.2017.12.038
15. I. Alessandri , E. Comini, E. Bontempi, G. Faglia, LE. Depero, G. Sberveglieri, *Sensors and Actuators, B: Chemical,* **128(1)**, 312(2007), **DOI:**10.1016/j.snb.2007.06.020
16. E. Comini, M. Ferroni, V. Guidi, A. Vomiero, P.G. Merli, V. Morandi, M. Sacerdoti, G. Della Mea, G. Sberveglieri, *Sensors and Actuators, B: Chemical,* **108(1)**, 21(2005), **DOI:**10.1016/j.snb.2004.10.041
17. M.C. Carotta, V. Guidi, C. Malagù, B. Vendemiati, A. Zanni, G. Martinelli, M. Sacerdoti, S. Licoccia, M. Luisa Di Vona, E. Traversa, *Sensors and Actuators, B: Chemical*, **108(1)**, 89(2005), **DOI:**10.1016/j.snb.2004.11.070
18. S. Cao, H. Chen, T. Han, C. Zhao, L. Peng, *Materials Letters,* **180**, 135(2016), **DOI:**10.1016/j.matlet.2016.05.105
19. I. Ganesh, A.K. Gupta, P.P. Kumar, P.S.C. Sekhar, K. Radha, G. Padmanabham, G. Sundararajan, *Materials Chemistry and Physics,* **135(1)**, 220(2012), **DOI:**10.1016/j.matchemphys.2012.04.062
20. H.Yu, S. Zhang, H. Zhao, G. Will, P. Liu, *Electrochimica Acta,* **54(4),** 1319(2009), **DOI:**10.1016/j.electacta.2008.09.025
21. R. Subasri, M. Tripathi, K. Murugan, J. Revathi, GVN. Rao, TN. Rao, *Materials Chemistry and Physics,* **124(1)**, 63(2010), **DOI:**10.1016/j.matchemphys.2010.08.013
22. L. Scandola, S. Latorrata, R. Matarrese, C. Cristiani, I. Nova, *Materials Chemistry and Physics* **234**,1(2019), **DOI:**10.1016/j.matchemphys.2019.05.074
23. L. Dhatchinamurthy, P. Thirumoorthy, L. Arunraja, S. Karthikeyan, *Materials Today: Proceedings, In Press* (2019), **DOI:**10.1016/j.matpr.2019.08.219
24. F. Mastali Khan, M. Rashidzadeh, A. Nemati, A. Irandoukht, B. Faridnia, *International Journal of Environmental Science and Technology*, **8(3)**, 545(2011), **DOI:**10.1007/bf03326240
25. Z. Wei, Q. Zhou, J. Wang , Z. Lu, L. Xu, W. Zeng, *Nanomaterials,* **7**, 1015(2019), **DOI:**10.3390/nano9071015

26. W. Zeng, Y. Li, B. Miao, L. Lin, Z. Wang, *Sensors and Actuators, B: Chemical,* **191**, 1(2014), **DOI:**10.1016/j.snb.2013.09.092
27. C. Wang , C. Feng, M. Wang, X. Li, P. Cheng, H. Zhang.Y. Sun, P. Sun, G. Lu, *RSC Advances* , **5(38)**, 29698(2015), **DOI:**10.1039/c5ra01121c
28. H. Song, L. Xia, X. Jia, W. Yang, *Journal of Alloys and Compounds,* **732**, 191(2018), **DOI:**10.1016/j.jallcom.2017.10.205
29. L. Song, Y. Li, S. Li, L. Liu, L. Wang, X. Guo, H. Lian, *Journal of Materials Science: Materials in Electronics,* **28(1)**, 652(2017), **DOI:**10.1007/s10854-016-5570-6
30. Q. Wang, C. Wang, H. Sun, P. Sun, Y. Wang, J. Lin, G. Lu, *Sensors and Actuators, B: Chemical,* **222** 257(2016), **DOI:**10.1016/j.snb.2015.07.115
31. C. Balamurugan, S.J. Song, H.S. Kim, *Journal of the Korean Ceramic Society,* **55(1)**, 1(2018), **DOI:**10.4191/kcers.2018.55.1.10
32. E.P. Wonohardjo, G.P. Kusuma, *Procedia Computer Science,* **157**, 638(2019), **DOI:**10.1016/j.procs.2019.08.224
33. S. Abraham, X. Li, International Journal of Wireless Information Networks, **23(1)**, 57(2016), **DOI:**10.1007/s10776-016-0299-y
34. R. Pitarma, G. Marques, B.R. Ferreira, *Journal of Medical Systems,* **41(2)**, 1(2017), **DOI:**10.1007/s10916-016-0667-2
35. R. Kingsy Grace, S. Manju, *Wireless Personal Communications,* **108(4)**, 2499(2019), **DOI:**10.1007/s11277-019-06535-3
36. M. Sharma, T. Maity, *Wireless Personal Communications,* **102(1)**, 149(2018), **DOI:**10.1007/s11277-018-5831-1
37. H.A. Mahmoud, K. Narasimharao, T.T. Ali, KMS. K,alil. *Nanoscale Research Letters,* **13(1)**, (2018), **DOI:**10.1186/s11671-018-2465-x
38. V.Y. Zenou, S. Bakardjieva, *Materials Characterization,* **144**, 287(2018), **DOI:**10.1016/j.matchar.2018.07.022
39. G. Xia, H. Liu, X. Zhao, X. Dong, S. Wang, X. Li, *Chemical Engineering Journal,* **370**, 1111(2019), **DOI:**10.1016/j.cej.2019.03.257
40. J. Yu, X, Zhao, JC. Yu, G. Zhong, J. Han, Q. Zhao, *Journal of Materials Science Letters,* **20(18)**, 1745(2001), **DOI:**10.1023/A:1012458411717
41. Y. Kotani, A. Matsuda, M. Tatsumisago, T. Minami , T. Umezawa , T .Kogure, *Journal of Sol-Gel Science and Technology,* **19(1-3)**, 585(2000), **DOI:**10.1023/A:1008709210723
42. O. Wiranwetchayan, S. Promnopat, T. Thongtem, A. Chaipanich, S. Thongtem, *Materials Chemistry and Physics,* **240**, 122219(2020), **DOI:**10.1016/j.matchemphys.2019.122219
43. Wagutu A.W, Yano K, Sato K, E. Park, Y. Iso, T. Isobe, *Scientific African.* Journal Pre-proof. **6,** e00203 (2019), **DOI:**10.1016/j.sciaf.2019.e00203
44. S. Devikala, P. Kamaraj, M. Arthanareeswari, *Materials Today: Proceedings* **5(2)**, 8678(2018), **DOI:**10.1016/j.matpr.2017.12.293
45. T. Lan, J. Tu, Q. Zou, X . Zeng, J. Zou, H. Huang, W. Wei, *Electrochimia Acta*, **319**,101(2019), **DOI:**10.1016/j.electacta.2019.06.152
46. A. Garzon, A, Roman A. C. Zuñiga-Islas , E. Quiroga-González. *Ceramics International,* **46(1)**,1137(2019), **DOI:**10.1016/j.ceramint.2019.09.082
47. F.M.K. Tehrani, M. Rashidzadeh, A. Nemati , A. Irandoukht , F. Faridnia., *International Journal of Environmental Science & Technology,* **8(3)**, 545(2011), **DOI:**10.1007/BF03326240
48. L. Zhang, B. Khan, P. Cheng, Y.H. Hu, *Catalysis Today*, **341, 21**(2020), **DOI:**10.1016/j.cattod.2018.06.049
49. A. Tolosana-Moranchel, J.A. Casas, A. Bahamonde, L. Pascual, L.I. Granone,d, J. Schneider, R. Dillert, D.W. Bahnemann, *Applied Catalysis B: Environmental,* **241**,375(2019), **DOI:**10.1016/j.apcatb.2018.09.070
50. G. Nagaraj, A. Dhayal Raj, A. Albert Irudayaraj, R.L. Josephine. *Optik*. **179**, 889(2019), **DOI:**10.1016/j.ijleo.2018.11.009
51. H. Ali, N. Ismail , M.S. Amin, M. Mekewi, *Journal of Solid State Electrochemistry,* **21(6)**,

1605(2017), **DOI:**10.1007/s10008-017-3523-5
52. J. Wang , B. Liu, K. Nakata, *Cuihua Xuebao/Chinese Journal of Catalysis,* **40(3)**, 403(2019), **DOI:**10.1016/S1872-2067(18)63174-2
53. J. Yu, J.C. Yu, M.K.P. Leung, W. Ho, B. Cheng, X. Zhao, J Zhao, *Journal of Catalysis,* **217(1),** 69(2003), **DOI:**10.1016/S0021-9517(03)00034-4
54. G.V. Khade, N.L. Gavade, M.B. Suwarnkar, M.J. Dhanavade, K.D. Sonawane, K.M. Garadkar, *Journal of Materials Science: Materials in Electronics*. **28(15),** 1(2017), **DOI:**10.1007/s10854-017-6883-9
55. P. Hermawan , H.D. Pranowo, I. Kartini, *Indonesian Journal of Chemistry*. **11(2)**, 135(2011), **DOI:**10.22146/ijc.21400
56. S. Mahajan, S. Jagtap, *Applied Materials Today,* **18**, 100483(2019), **DOI:**10.1016/j.apmt.2019.100483
57. Y. Luo, C. Zhang, B. Zheng, X. Geng, M. Debliquy, *International Journal of Hydrogen Energy*. **42(31)**,20386(2017), **DOI:**10.1016/j.ijhydene.2017.06.066

[RJC-5720/2020]

Jurnal Ni-dipend TiO2

ORIGINALITY REPORT

20%	17%	15%	3%
SIMILARITY INDEX	INTERNET SOURCES	PUBLICATIONS	STUDENT PAPERS

MATCH ALL SOURCES (ONLY SELECTED SOURCE PRINTED)

5%

★ F. Mastali Khan Tehrani, M. Rashidzadeh, A. Nemati, A. Irandoukht, B. Faridnia. "Characterization and photocatalytic activities of nanosized titanium dioxide thin films", International Journal of Environmental Science & Technology, 2011

Publication

Exclude quotes	On	Exclude matches	< 5 words
Exclude bibliography	On		